Structure of the cholesteric focal conic domains at the free surface

R. Meister, M.-A. Hallé, H. Dumoulin, and P. Pieranski
Université Paris Sud, Laboratoire de Physique des Solides, Bâtiment 510, F-91405 Orsay, France
(Received 25 September 1995; revised manuscript received 21 June 1996)

Atomic force microscope examinations of the free surface and of microtome cuts of a cholesteric oligomer are reported. The obtained images lead to a model of the structure of cholesteric focal conic domains that appear spontaneously at the free surface. These domains develop in order to fulfill the boundary condition at the free surface together with a planar bulk texture. Estimations of the free energy confirm this model. [S1063-651X(96)04110-4]

PACS number(s): 61.30.−v, 61.16.−d, 68.10.−m

I. INTRODUCTION

Atomic force microscope (AFM) [1] investigations are useful methods of exploring surfaces that are not flat, especially in the case where the resolution of optical methods is not sufficiently high. In this regard, liquid crystal phases are interesting topics because they can have nonplanar surface structures that are very small in amplitude. An example shown by de Gennes [2] is a periodic system of grooves and hills that should appear at the free surfaces of nematic liquid crystals with homeotropic boundary condition submitted to a horizontal magnetic field. Another example of surfaces that are not flat are liquid crystals where defect lines start and/or end at the free surface. These reliefs have been successfully examined by AFM [3]. There exist also investigations on smectic phases [4,5].

Cholesteric phases show a very great manifold of possible surface structures [6], depending on several parameters, such as the thickness of the liquid crystal layer and the thermal treatment of the sample. The topology of the system cholesteric plus homeotropic boundary condition requires the introduction of systems of disclinations. These can be arranged in several ways, leading to the great number of different structures. In particular, a double-spiral conical relief corresponding to a focal-conic texture was observed [6] (see Fig. 1).

In all these examples the investigated material had to be sufficiently stiff in order to be examined by AFM methods. But with the synthesis of new oligomer and polymer substances a number of useful samples are available. The material usually possesses a glass transition at elevated temperature and can be investigated in the frozen state at room temperature without difficulty. But even swallow-tailed molecules can be successfully examined in their smectic states [5]. This is due to the ''tapping mode'' (registered trademark of Digital Instruments) of the AFM where the probing tip is placed at the end of a vibrating cantilever. The sample interacts with the tip only when the cantilever is at the lowest position of the vibration cycle. By this the interaction energy is reduced to a minimum.

A method of getting information about the bulk structure of mesophases is via microtome cuts or freeze fractures. The samples can be examined by polarization microscopy [7,8] or electron microscopy [9–12]. But surfaces produced by a freeze fracture process are known to possess a relief due to the anisotropic propagation of the fracture [13] and also surfaces created by the action of a microtome knife in quenched liquid crystals have a topography that depends on the texture of the cut material. Therefore, the microtome cuts can be explored by AFM. Examples of these investigations are cholesteric [11] and blue phases [14].

In this article we will report about AFM investigations of the free surface and of microtome cuts of a cholesteric oligomer. These two surfaces give complementary information on the cholesteric texture and allow us to resolve the three-dimensional structure of the cholesteric focal-conic domains.

II. EXPERIMENT

In our examinations we used the following siloxan oligomer supplied by Wacker Chemie, Germany via J.-M. Gilli ($3 \leqslant n+m \leqslant 7$):

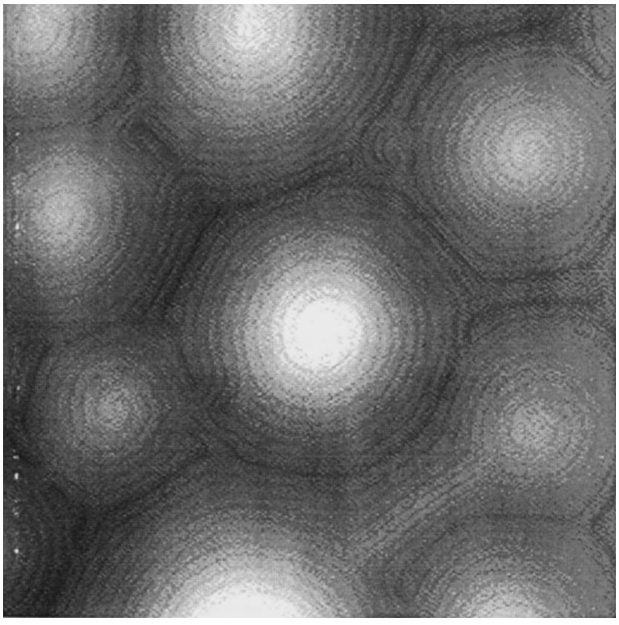

FIG. 1. An AFM image of the free surface of the cholesteric focal-conic domains at the free surface. All double spirals show the same sense of rotation and possess a conical form with the center at the highest position (image length 10 381 nm).

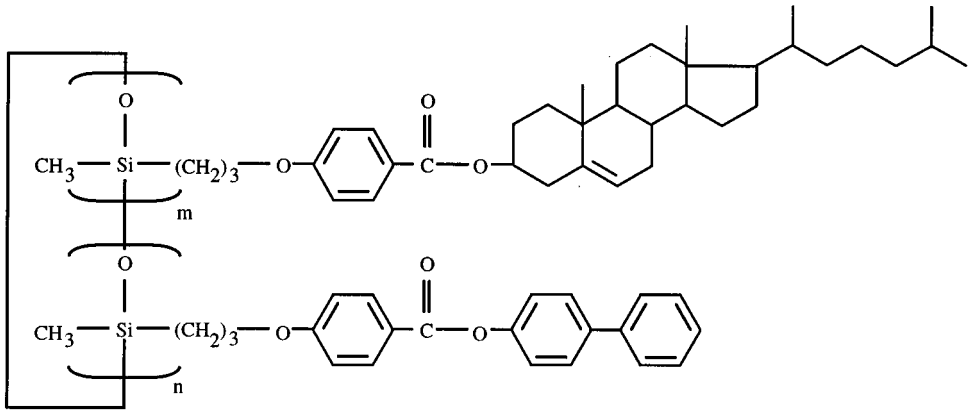

glassy state $\overset{50^\circ C}{\longleftrightarrow}$ Chol $\overset{195^\circ C}{\longleftrightarrow}$ BP I, II, III $\overset{198^\circ C}{\longleftrightarrow}$ Iso

The ratio of the two different mesogenic side chains attached to the cyclic structure controls the helical pitch. Our experimental work is based on that oligomer with an equal ratio of the chiral and the achiral side chain. The half helical pitch of this material is 145 nm [15]. Note the glass transition at 50 °C that allows us to investigate the cholesteric phase with the AFM in the rigid glassy state.

In order to produce the focal-conic surface structure the substance was put onto a substrate and heated to 120 °C. By means of shearing the cholesteric phase was orientated into a planar configuration. The focal conic surface structure developed spontaneously at the free surface while the sample was placed for 2 min in an oven at 140 °C. After taking the sample out of the oven and letting the temperature decrease to room temperature, the focal conic surface structure was frozen in the glassy state.

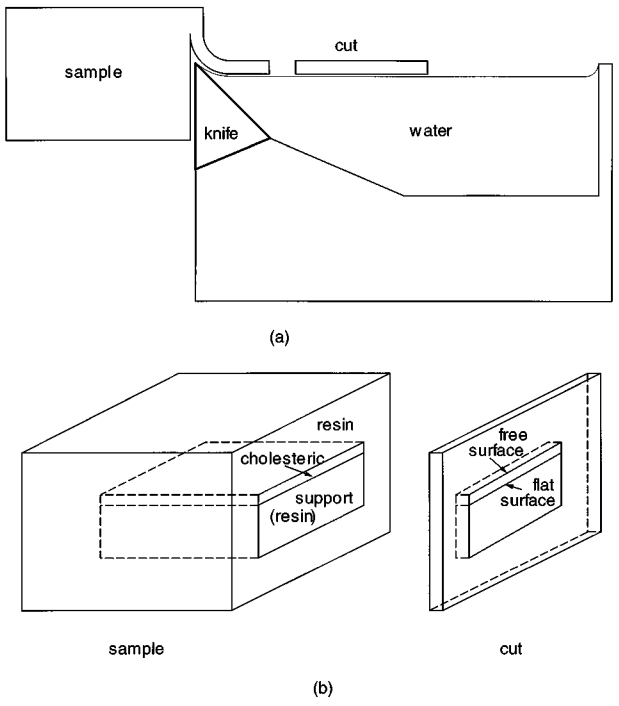

FIG. 2. (a) Schematic representation of the microtome cut process. The sample is cut by a diamant edge and the cuts float on the water surface after the cut. Only the upper sides of the cuts were examined in our experiments. (b) The geometry of the samples. There are two surfaces cut by the microtome knife: the free surface, covered with Araldite to suppress convolution effects, and the flat surface cholesteric/support.

The exploration of the free surface was made with glass as support. It showed a planar boundary condition, which is favorable with respect to the intermediate structure of the sample.

In order to be cut by a microtome, the support for these samples cannot be glass, but has to be a material that can be easily cut. Therefore we used ''Araldite,'' a commercial resin especially optimized for microtome use. The boundary conditions are not as simple as with glass. The resulting structure of the flat surface cholesteric/resin depends (like the free surface) on several parameters, such as the thickness of the liquid crystal layer, the rubbing of the substrate, and the thermal treatment of the sample. But as the time scale of the transformations to the preferred state is rather long, we arrived at samples that showed the focal-conic structure at the free surface, while the boundary at the other surface was still planar.

The samples were prepared in the following way: Flat resin plates were made by polymerizing it between two parallel glass plates at 60 °C for 2 d. Afterwards, the cholesteric phase was put on these flat supports. The whole sample was then put into a compact block of (still liquid) resin and this was once again polymerized at 60 °C for 2 d.

The samples were cut with a microtome either perpendicular or oblique to the free surface. The thickness of the cuts varied between approximately 70 nm and 140 nm (see Fig. 2).

III. RESULTS

A. Free surface

The surface of the cholesteric focal conic domains is shown in Fig. 1. The helix axis lies more or less parallel to

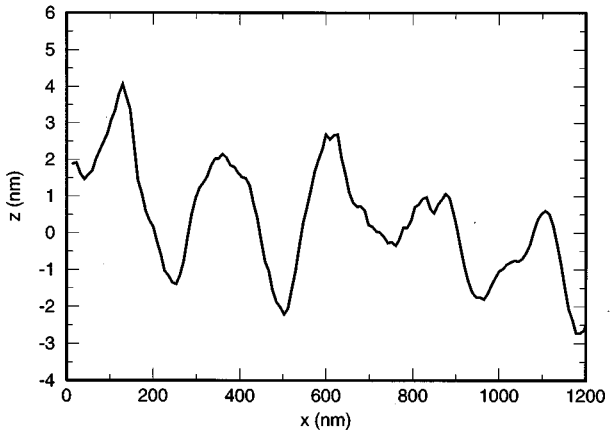

FIG. 3. A section of the surface structure due to the helical twist. Note that the length scale of the z axis is considerably smaller than that of the x axis.

the free surface, giving rise to a surface structure whose periodicity is 195 nm, comparable to the half helical pitch. A relief is shown in Fig. 3; the height is about 4 nm, leading to a mean slope of 2°. The form of the top region is different from that of the bottom, showing different radii of curvature. In the focal conic structure the ''cholesteric (half-) planes'' are arranged in the form of a double spiral, ending in the center of the spiral. Here two defect lines approach the surface, either two λ^+ or two τ^+ lines.

For thin samples, the diameter of the spiral is (roughly) proportional to the thickness of the liquid crystal layer. But if the height of the layer is sufficiently large, there seems to be a maximal value of the spiral diameter. A section through the center of the helix (Fig. 4) reveals that the three-dimensional surface is a cone, whose diameter is (in this case) 5 μm, and whose height is 9 nm, which results in an average slope of 1°.

Note that in Fig. 1 the two curves of the crests finish at the top of the cone while the groove line is continuous. Note also that all spirals possess the same sense of rotation.

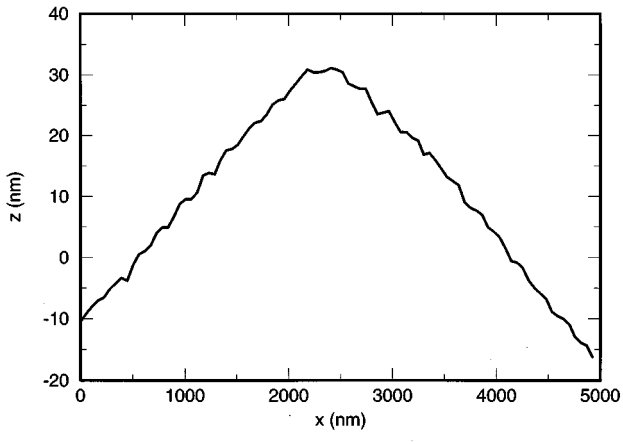

FIG. 4. A section of the cholesteric focal-conic domains, cut through the center of the cone. The periodic structure due to the cholesteric pitch is superimposed on the conical form. Note that the length scale of the z axis is considerably smaller than that of the x axis.

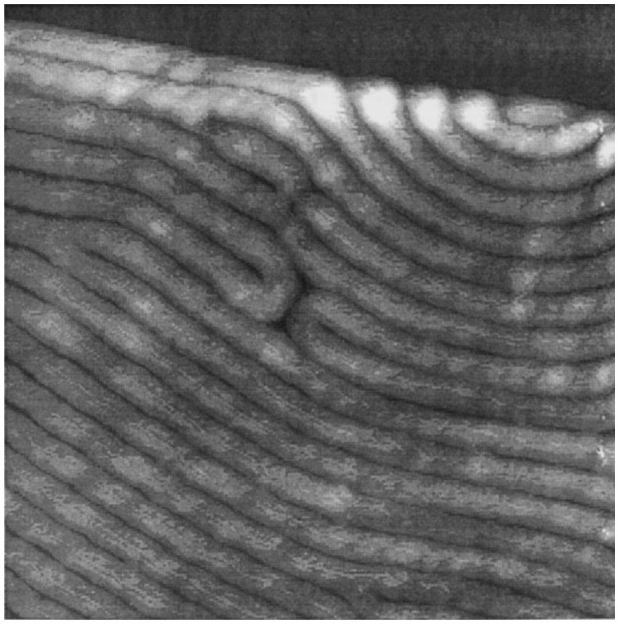

FIG. 5. An AFM image of a microtome cut, perpendicular to the free surface. The image shows the interface cholesteric/air (the free surface). Note that the sample is embedded in Araldite so that the image actually shows the interface cholesteric/resin. The structure of the cholesteric phase has not changed during this covering process, however. The image shows the oblique orientation of the helix axis relative to the free surface (image length 2407 nm).

B. Perpendicular microtome cut

A microtome cut of the cholesteric phase is shown in Fig. 5. The relief due to the cholesteric pitch is quite semblant to that of the free surface, although it is obtained by a totally different process. The height of this relief depends on the thickness of the microtome cuts; the thinner the cuts are the greater the structure becomes. A section is given in Fig. 6, showing that here the mean height is about 8 nm, while the

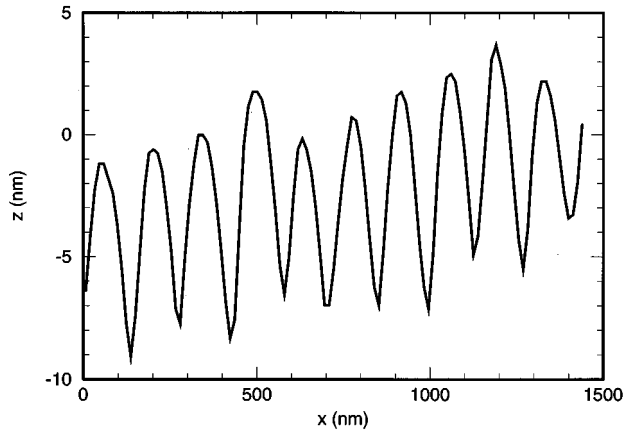

FIG. 6. A section of the cut surface. The profile height is greater than in Fig. 3, so that here convolution effects are probably of greater importance. Note that the length scale of the z axis is considerably smaller than that of the x axis.

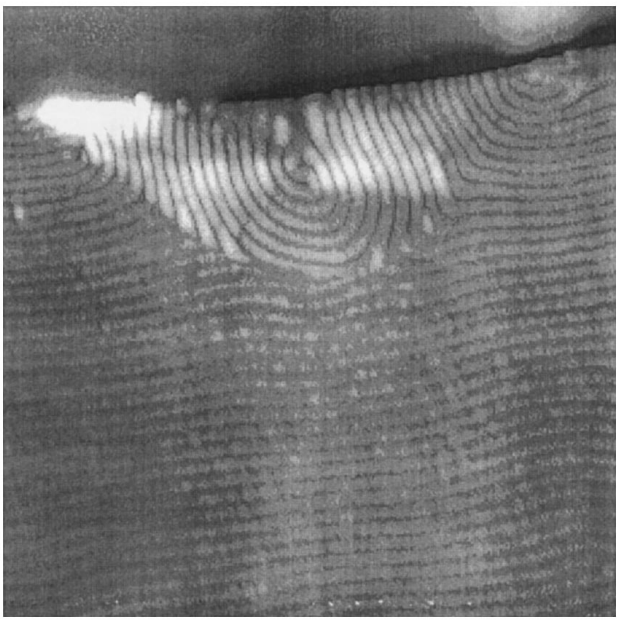

FIG. 7. An AFM image of a microtome cut, oblique to the free surface. The image shows a cut through a focal conic domain, embedded in the planar bulk texture (image length 7000 nm).

periodicity is 145 nm, being equal to the half cholesteric pitch. This yields an average angle of 6°. Again, the summits and valleys show different radii of curvature.

The given periodicity is the minimal value found. Of course every periodicity greater than the half helical pitch can be observed if the helical axis is not in the plane of the cut.

C. Microtome cuts oblique to the free surface

An image of this kind of cut is shown in Fig. 7. The spiral arrangement of the cholesteric planes in the region of the focal conic domain is clearly visible. The bulk phase is still in a planar texture, the periodicity being 174 nm, giving an approximation for the angle of inclination of 33°, which is in very good agreement with the estimated value of 30°.

Contrary to the situation at the free surface, here two groove lines end in the center of the spiral, while the crest line is continuous. The correspondence between crests and grooves to perpendicular and parallel orientations of **n** with respect to the surface is therefore inverse to the situation at the free surface. Note how the focal conic domain is embedded in the planar texture. The helix axis of those cholesteric planes that lie between the free surface and the center of the spiral makes a greater angle with the plane of the cut than the helix axis of those planes that lie on the opposite side of the center (still in the region of the focal conic domain).

IV. DISCUSSION

A. Notations ''helix axis'' and ''cholesteric planes''

A helical twist axis for cholesteric phases has been defined by several authors, e.g., an implicit vector equation [16]:

$$\mathbf{n}\times(\mathbf{u}\cdot\boldsymbol{\nabla})\mathbf{n}=(2\pi/p)(\mathbf{u}\cdot\mathbf{t})\mathbf{t}, \tag{1}$$

where **u** is an arbitrary vector and **t** is a unit vector in the direction of the twist axis. Another definition declares the helix axis as the eigenaxis with the greatest eigenvalue of the (two-dimensional) twist tensor [17].

Describing the cholesteric phases by two vector fields perpendicular to each other ($\mathbf{n}\cdot\mathbf{t}=0$) gives some interesting relation to biaxial nematics and allows a simple classification of the three defect types in cholesterics. Using a third vector $\mathbf{o}=\mathbf{n}\times\mathbf{t}$, the defects are classified as follows:

χ: **t** is continuous, **n** and **o** are discontinuous

λ: **n** is continuous, **t** and **o** are discontinuous

τ: **o** is continuous, **n** and **t** are discontinuous.

However the symmetric definition of the three types of defects does not imply equal distortion energies for the defects.

Although it is sometimes very useful to consider the helix axis field as a second vector field which helps in understanding the structure of cholesteric phases, we want to stress that there is in principle no need for the definition of a twist axis, because the knowledge of $\mathbf{n}(\mathbf{r})$ alone is sufficient to describe the cholesteric phase. Another point is that in some circumstances the twist axis cannot be defined unambigiously [18], for example, in a cholesteric that is completely unwound by external forces (there is no twist at all) or at the center of the double twist cylinders, considered in relation to the blue phases (here the twist is equal in every direction perpendicular to **n**). Analogous comments apply to the notion of cholesteric planes. Neither do we imply any layered structure, nor any relation between the cholesteric planes at two different points that results in a classification of the two points as ''belonging to the same'' or ''belonging to different planes.''

We will use the notions ''cholesteric planes'' and ''helix axis'' only in those circumstances where a helix axis can be defined without any difficulty by either of the two above definitions (i.e., configurations that do not deviate strongly from the ideal cholesteric structure) and this only to avoid otherwise clumsy formulations.

A cautionary remark shall also be made on the standard figures of the τ and λ defects and their combinations in pairs. The usual images do not give a general director distribution. The twist axes in these pictures always lie in the figure plane. Here the observation of an ''additional plane'' is directly related to the defects. In our opinion, the one-to-one relationship between the additional plane and defects is no longer fulfilled in the general case. Both the director and the twist field may be continuous and there are no defects, even if a ''new plane'' seems to appear. The consideration of a cholesteric as a sort of layered system is sometimes very misleading.

In the following figures which show director distributions we will use the convention in which the tips of the pins are oriented towards the observer. This convention is especially important for the imagination of two different cuts of the same three-dimensional director distribution.

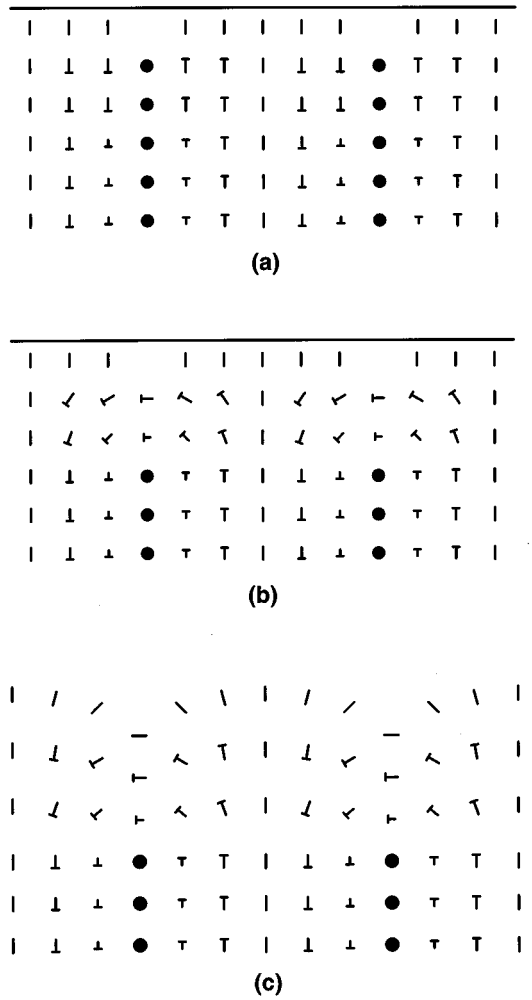

FIG. 8. A cholesteric phase with homeotropic boundary conditions: (a) The director rests in a plane. This is not compatible with the molecular field [20]. (b) The director turns out of the plane in order to fulfill the molecular field requirements [20]. (c) The director distribution at the free surface. The equilibrium relief results from the competition between the surface energy and the bulk free energy.

B. Periodic surface relief due to the cholesteric helix

In this article we do not attempt to give a complete discussion of this relief, which is done in [19], but we want to present a qualitative description of the resulting director distribution that is necessary to develop the focal-conic structure that follows in Sec. IV C. Let us begin with the consideration of a flat surface with homeotropic boundary conditions [20]. A first attempt to sketch the director distribution is shown in Fig. 8(a). But this is not the real situation, because it does not fulfill the molecular field requirements. Figure 8(b) shows a structure that is compatible with the molecular field [20]. If now the boundary conditions are altered in order to allow for a free surface, the system can reduce its free energy. The equilibrium relief results from the competition between the surface energy and the bulk free energy. The proposed structure is sketched in Fig. 8(c).

The real situation is more complex because of the greater periodicity of the free surface structure (195 nm), compared to the helical pitch (145 nm), but for the following it will be sufficient to describe the surface boundary by a phenomenological preferred oblique orientation of the helix axis relative to the surface (see Fig. 5):

$$f_f = -k_f(\mathbf{t}\cdot\mathbf{s})^2 \quad \text{or} \quad f_f = -k_f \cos^2(\xi-\xi_0), \tag{2}$$

where **t** is the helix axis and **s** is the preferred surface orientation of the cholesteric.

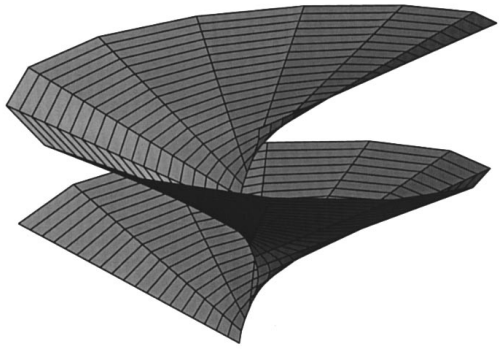

FIG. 9. A three-dimensional surface representing the distribution of the cholesteric planes in the cholesteric focal-conic domain at the free surface [this sketch shows a surface $z' = \text{const}$ of Eq. (8)].

C. Model I

In the description of model I we will begin to discuss the bulk structure of the focal-conic domain and then take a closer look at the center of the spiral and on the border between the focal-conic and the planar domains.

The cholesteric planes are arranged in the form of a cone with a superimposed spiral structure. A three-dimensional surface representing one cholesteric plane is shown in Fig. 9. A section through the center is given in Fig. 10, showing an inclination of the planes by the angle α. Due to the continuous screw axis (Fig. 9), a half plane with index 1 appears after a rotation of π, translated by $p_h/2$, on the other side of the center so that the whole structure can be generated starting from two half planes. Indeed, a cut perpendicular to the cone axis (the free surface in Fig. 1) reveals two cholesteric planes.

From the discussion in Sec. IV B it follows that the two defect lines are of the λ^+ type. In the bulk these lines wind around each other like two twisted threads. Figure 11 shows the director distribution in the xy plane. This plane cuts the two defect lines. The cholesteric planes are inclined by the angle $0<\alpha<\pi/2$. A cut containing the central axis is shown in Fig. 12, representing a rather complex distribution.

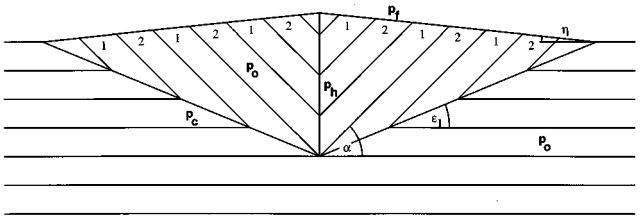

FIG. 10. Model of the cholesteric focal conic domains. The figure shows a cut along the center of the cone. Note that the exact structure of the center is neglected in this sketch.

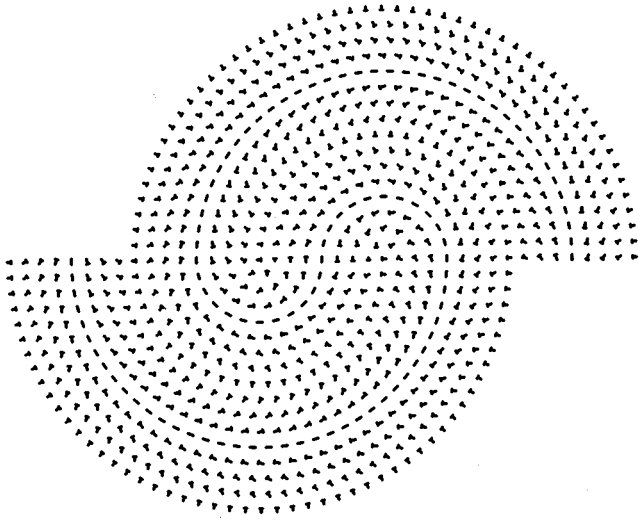

FIG. 11. Director distribution of a double spiral possessing two λ^+ defects. The helix axis makes an angle $90°-\alpha$ with the figure plane, i.e., the cholesteric planes are inclined with respect to the center.

Far away from the center the cholesteric planes are clearly visible, but if the center is approached this notion becomes somewhat diffuse because twist deformations exist in several directions. If we look exactly at the center there is again a twist axis that is fairly visible. Here are two points to note: the periodicity is not p_0 but $p_h=p_0/\cos\alpha$ due to the inclination of the cholesteric; and the twist sense is the same as for the undistorted phase.

The two defect lines of λ^+ type are regularly cut by this plane, although they are not clearly visible. This is not really surprising because this sort of defect shows no discontinuity in **n**, only for the twist **t**.

Let us now look at the embedding of the focal conic domain in the bulk planar texture. As the periodicities along the z axis are different (p_h vs p_0), the surface between the two domains cannot be arbitrary, but has to fulfill a geometric constraint. As can be seen in Fig. 10, the cholesteric planes of the two respective domains can adapt themselves if the slope of the domain border is $\epsilon_1=\alpha/2$. The exact director

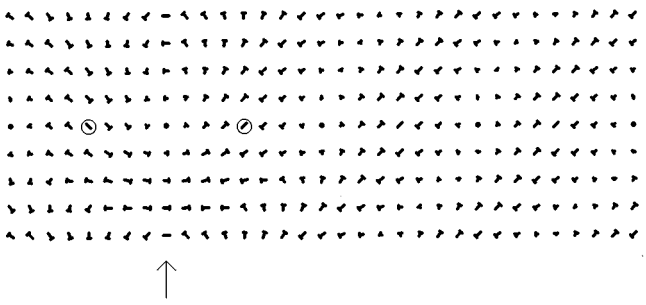

FIG. 12. The director distribution in the plane of Fig. 10 (perpendicular to Fig. 11) that contains the central axis of the cone (marked in the figure). The two entangled λ^+ defects lines cross this plane regularly and are also marked. Note that the director in the central axis is twisted along this axis, with periodicity p_h.

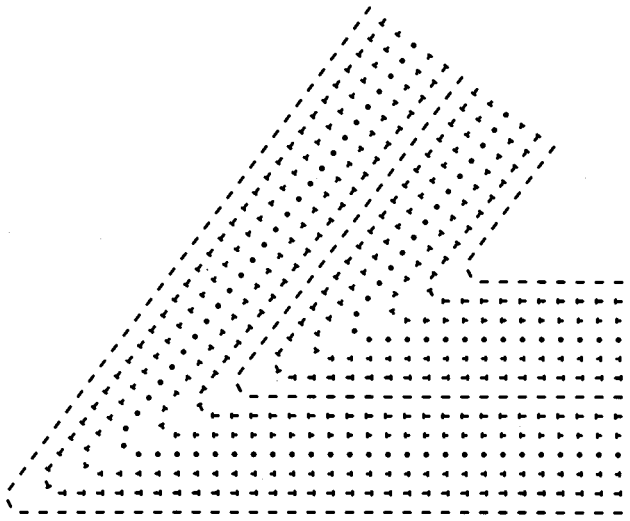

FIG. 13. The director distribution at the border between the two domains. The director field is continuous, but possesses the helical pitch $p_c=p_o/\cos(\alpha/2)$ at the border.

distribution of the border is sketched in Fig. 13. Note that the periodicity along the cone border is neither p_0 nor p_h but $p_c=p_0/\cos(\alpha/2)$. Figure 14 shows the director field along a circle around the center of the cone at constant height, not following the screw axis. Due to this axis, the director distribution does not possess a circular symmetry. It can easily be seen that there exists no difficulty for the director to be fit into the planar structure that is sketched in the outer circle. Therefore, there are no discontinuities in the director field. Neither is there a discontinuity in the twist field (which indeed possesses in both domains a cylindrical symmetry), so that there are no disclinations on the domain border.

As defect lines cannot simply stop in the bulk phase, we must conclude that the two λ^+ lines meet at the lowest point

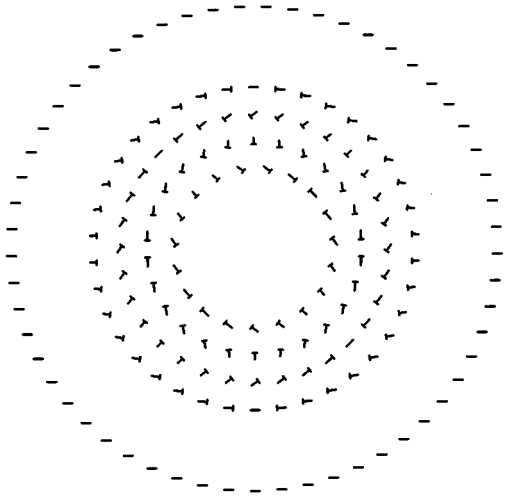

FIG. 14. Director distribution at the border between the two domains, cut perpendicular to the cone axis. The index of the sum of the two λ^+ lines is $S=0$. The focal-conic domain can adapt itself without singularity to the outer planar texture, which is sketched in the outer circle.

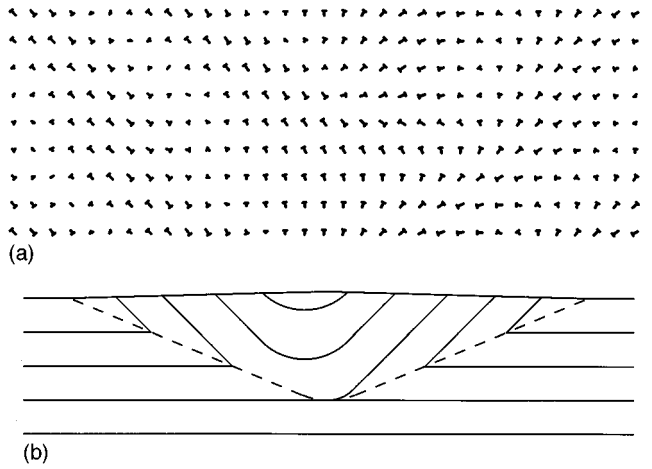

FIG. 15. (a) Director distribution of a plane parallel to the one in Fig. 12, but at a distance $d>p_0/4$. The plane shown does not contain the central axis. The two λ defects are not cut by this plane, either. (b) The same plane as in (a), but here the cholesteric planes are sketched. The appearance of an additional plane does not imply defects on the cone border.

of the focal conic domain, i.e., there is only one defect line entwined around itself, starting and ending at the surface, in the center of the cone.

An example of how complex the director distribution can become is given in Fig. 15(a), which shows a vertical cut parallel to the central axis but at a distance $d>p_0/4$ away from it. While the cholesteric structure is fairly visible in the right- and left-hand parts of the figure (cholesteric planes), it is complicated in the central part, although the cut shows a region far away from the center. This complexity is due to the fact that the helix axis does not make a constant angle with the figure plane. While **t** is (more or less) parallel to the figure plane at the right- and left-hand sides of the picture, it includes the angle α with it in the middle part. Note that one plane at a definite height z at the right figure border is, when following the cholesteric plane, transferred to a height $z+p_h/2$ at the left border. Figure 15(b) shows the same cut, but in the notation of cholesteric planes. If the conical cholesteric structure is cut parallel to the center, the form of the cholesteric planes is that of hyperbolas, although slightly deformed through the superimposed spiral structure. The screw axis seems to introduce a new plane on the left-hand side of Fig. 15(b), implying some defects. Following the above arguing there are no defects, thus demonstrating that the pictural description of a cholesteric phase as a layered structure is indeed misleading.

D. Alternatives

There exists a further possibility for constructing a helical cone resulting in a spiral surface structure. Beginning with the spiral in Fig. 11, we could have changed the rotation sense of the screw axis.

The cholesteric is arranged in a way similar to our first model, i.e., the planes are inclined by the angle α with respect to the planar texture. Yet the structure is different from the first model. The rotation sense of the surface spiral has changed, as has the rotation sense of the twist deformation in the center of the spiral, which is certainly unfavorable with respect to energetic considerations. This can be seen in Fig. 16 showing a cut along the central cone axis. The structure of the border of the two domains is also altered (see Fig. 17). Disclination lines have to appear on the surface in this director configuration.

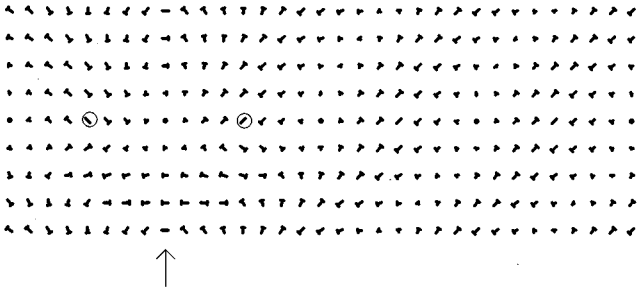

FIG. 16. The director distribution in a plane that contains the central axis. In this figure the rotation sense of the screw axis is reversed, resulting in a different director distribution as in Fig. 12. The twist sense at the center is inverse to the molecular twist.

Given the focal conic and the planar domains, we can construct a second possible orientation II of the two structures by turning the focal cone through π around a horizontal axis. This is shown in Fig. 18. The spiral rotation sense at the surface has changed. Note, however, that the slope angle of the domain border is given by $\epsilon_{II}=(\pi-\alpha)/2$ and that therefore the focal-conic domain has a different shape, while in the first model the cone was flat, we now have a peaked cone. Note that this structure yields the same surface angle of the helix axis **t** (neglecting the small height of the cone at the free surface). However, we can exclude this structure by experimental evidence. Imagine an oblique cut through the two structures shown (Figs. 10 and 18). Only in the first case, the angle between the helix axis and the cut plane is in accor-

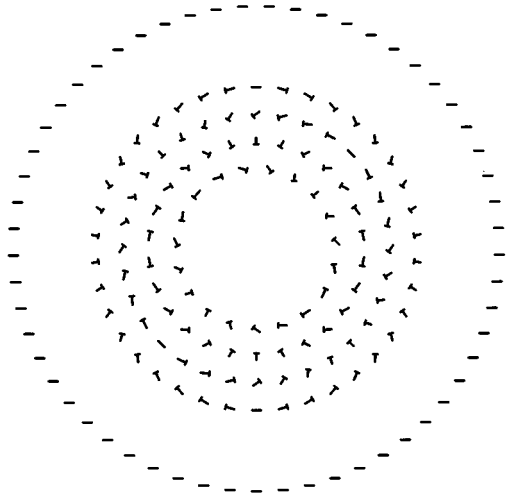

FIG. 17. Director distribution at the border between the two domains, cut perpendicular to the cone axis, for the case of the inverted rotation sense. The defect index is $S=2$. The focal-conic domain cannot adapt itself without additional singularities to the outer planar texture which is sketched in the outer circle.

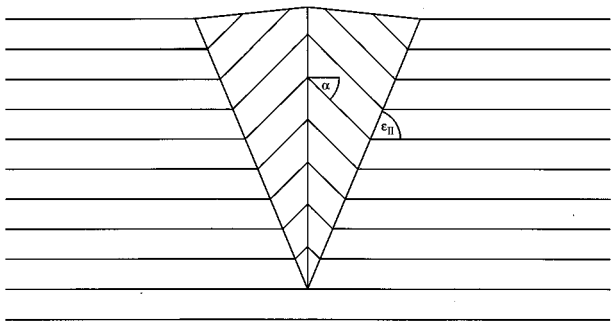

FIG. 18. A second possibility to fit a focal-conic domain in the planar structure. Note that the form of the cone is different from that in Fig. 10 although the helix axis makes the same angle with the free surface, if one neglects the very flat cone of the free surface.

dance with the experimental situation, i.e., is greater in the region between the free surface and the center than in the other region (cf. Sec. III C). Energetic estimations will also give some evidence for the exclusion of the second structure.

E. Helicoidal generation of pairs

A helicoidal arrangement of defect lines has already been considered in detail in [21,22], whose structure is generated by turning a two-dimensional pattern around a screw axis. For reasons of continuity, the periodicity of the screw axis is an integer multiple of the half helical pitch,

$$p = 1/2 m p_0, \tag{3}$$

where m is taken to be positive if the rotation sense of the screw axis is the same as that for the molecular twist. It can easily be shown that the resulting defect is a χ line of index

$$S = 1 - \tfrac{1}{2} m. \tag{4}$$

Note that there exist no defects for $m=2$. The center of the defects can be dissociated in pairs of (λ,τ) defect lines, turning in a helix around the central axis, and various combinations of different periodicities inside and outside of the central region can be constructed [21,22].

Thus our model resembles the above structures, which we can identify with the case $m=2$, $S=0$ (and $m=-2$, $S=2$ for the case of the inverse screw axis). The two-dimensional patterns generated can be seen in Figs. 12 and 16. The additional inclination of the planes change the periodicity of the central region to

$$\tfrac{1}{2} p_h = \frac{m p_0}{2 \cos \alpha}. \tag{5}$$

Naturally, our model does not yield an undisturbed cholesteric for $m=2$ because $\alpha \neq 0$, but the structure resembles it most (cf. Fig. 14). Note that we arrive at the expected index $S=0$, if we follow the director distribution on the circle, but a value $S=2$ results from Fig. 17 for $m=-2$.

The starting disclinations are in both cases two λ^+ lines but the combination of the two defects is different. This might be interpreted in terms of homotopy group theory [23]. The combination of two line defects in media with non-Abelian fundamental groups can yield different results, depending on how the two defects are surrounded by a loop with respect to a third defect line. As in our case there is no third defect, the reason for the two different results seems to be the way in which the two defect lines are twisted around each other. This means that we have to bring in a χ defect of index $S=2$ from infinity to deform the two helicoidal arrangements with different helix rotation sense into one another. In any case, the two values $S=0$ and $S=2$ are consistent with the results that can be read from the class multiplication table for cholesteric defects [24].

Experimental investigations of pairs of twisted defects were already made in [25,26]. For some combinations, the two defect lines were topologically not equivalent, even if they were of the same type. However, for our case the two lines are equivalent, showing again the great variety of possible structures of the cholesteric phase.

F. Energetic estimations

In general, the structure of a mesogenic phase should result from the minimization of the free energy. But this is already quite complex for nematics unless the one-constant approximation is used or the director is constrained to lie in a plane. For cholesteric phases, this becomes still more difficult due to the twisted structure. Therefore, we will not try to extract the free energy from first principles but give some estimations concerning the model.

To begin with the bulk energy, let us assume for the director distribution (see Fig. 10)

$$\mathbf{n} = \begin{pmatrix} \cos\alpha \cos\phi \cos\theta - \sin\phi \sin\theta \\ \cos\alpha \sin\phi \cos\theta + \cos\phi \sin\theta \\ \sin\alpha \cos\theta \end{pmatrix}, \tag{6}$$

where α is the angle of inclination, ϕ the azimuthal angle, and θ the angle describing the helical twist, whose value is given by

$$\theta = \frac{2\pi}{p_h} z', \tag{7}$$

$$z' = z - r \tan\alpha - \frac{m p_h}{2}(2\pi - \phi), \tag{8}$$

$$\phi = \arctan(y/x), \tag{9}$$

$$r = \sqrt{x^2 + y^2}. \tag{10}$$

Note that $z'=\text{const}$ is an implicit equation for the cholesteric planes of Fig. 9. The gradient terms for the three types of elastic deformation are obtained from this director distribution. After some lengthy calculations we arrive at

$$(\nabla \cdot \mathbf{n})^2 = \frac{(m-2)^2 \cos^2\theta \cos^2\alpha}{4r^2}, \tag{11}$$

$$(\mathbf{n} \cdot \nabla \times \mathbf{n} - 2\pi/p_0)^2 = \frac{\sin^2\theta \sin^2\alpha}{4r^2}, \tag{12}$$

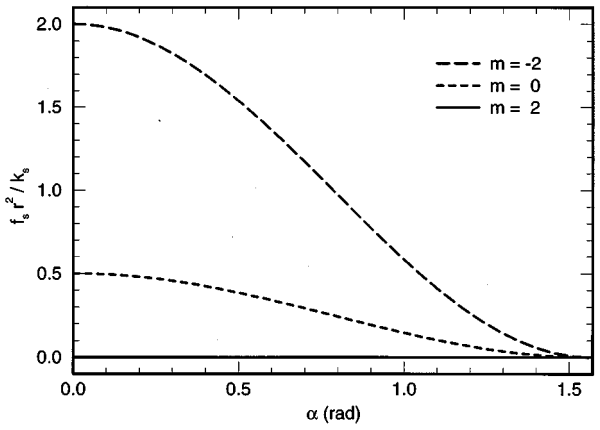

FIG. 19. Plot $f_s r^2/k_s = f(\alpha)$ [Eq. (11)] showing the dependence of the splay deformation free energy density on the angle α. The parameter m determines the periodicity of the screw axis.

$$(\mathbf{n}\times\nabla\times\mathbf{n})^2=\frac{4\sin^4\theta\sin^2\alpha+(m-2)^2\sin^2\theta\cos^2\alpha}{4r^2}. \tag{13}$$

To eliminate the dependence on θ, the distortions are averaged over the periodicity p_h along the z axis. Due to the symmetry of the problem, the dependence on the azimuthal angle ϕ (via θ) vanishes, too.

$$f_s=k_s(\nabla\cdot\mathbf{n})^2=k_s\frac{(m-2)^2\cos^2\alpha}{8r^2}, \tag{14}$$

$$f_t=k_t(\mathbf{n}\cdot\nabla\times\mathbf{n}-2\pi/p_0)^2=k_t\frac{\sin^2\alpha}{8r^2}, \tag{15}$$

$$f_b=k_b(\mathbf{n}\times\nabla\times\mathbf{n})^2=k_b\frac{3\sin^2\alpha+(m-2)^2\cos^2\alpha}{8r^2}. \tag{16}$$

The dependences of the deformation energies on α are shown in the Figs. 19 (splay), 20 (twist), and 21 (bend). For

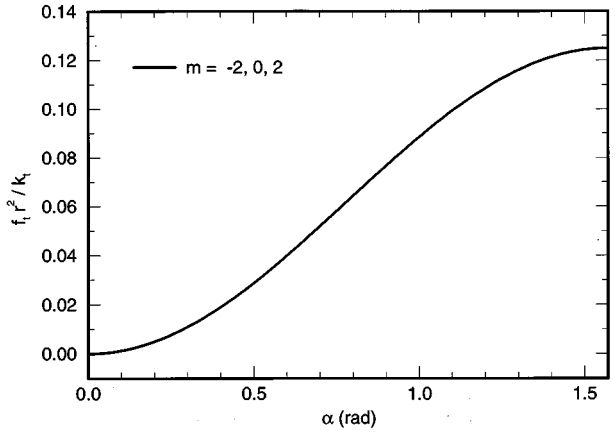

FIG. 20. Plot $f_t r^2/k_t = f(\alpha)$ [Eq. (12)] showing the dependence of the twist deformation free energy density on the angle α. The parameter m determines the periodicity of the screw axis.

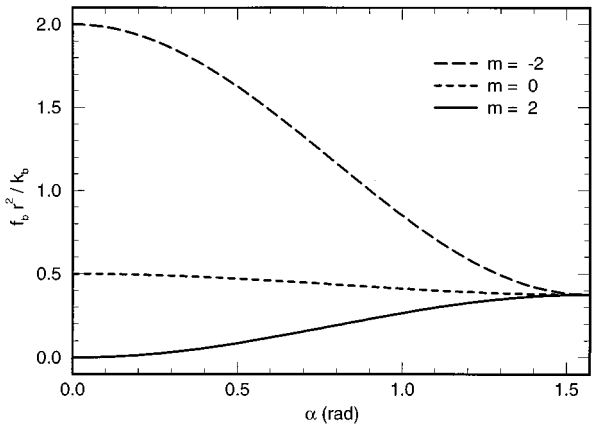

FIG. 21. Plot $f_b r^2/k_b = f(\alpha)$ [Eq. (13)] showing the dependence of the bend deformation free energy density on the angle α. The parameter m determines the periodicity of the screw axis.

$m=1$, 2, and 3 the full free energy density is lower for small angles α, while for the other values of m the situation is inverse, for usual values of k_s, k_t, and k_b. Note that the distortion energy is zero in the case of $m=2$ and $\alpha=0$, because this corresponds to the ideal cholesteric.

Comparing the free energies for $m=2$ and $m=-2$, it can be seen that the inversion of the screw axis rotation sense not only alters the center of the cone but also results in a different energetic situation.

In the following we shall only consider the situation $m=2$. The bulk energy density can in this case be written as

$$f_i=k_i\frac{\sin^2\alpha}{r^2}, \tag{17}$$

where $k_i=1/8k_t+3/8k_b$, while there is no splay deformation.

An additional distortion energy appears on the border between the focal-conic and the planar domains because the cholesteric planes are bent (see Fig. 13). Numerical calculations [19] lead to the following approximation:

$$f_c=k_c(p_c/p_0-1)^2, \tag{18}$$

where k_c is an effective elastic constant that can in principle be derived from the values of k_t, k_b, and p_0.

As the director distribution in the center of the cone is rather complex, we can only give an assumption, similar to Eq. (18), using as an indication the helical twist in the center of the cone:

$$f_h=k_h(p_h/p_0-1)^2. \tag{19}$$

The two situations of Figs. 10 (model I) and 18 (model II) possess the same bulk energy density f_i, but the geometrical dimensions are different. Neglecting again the very flat conical shape of the free surface, the height of the cone is given by (k=I,II):

$$h_k=r\tan\epsilon_k \tag{20}$$

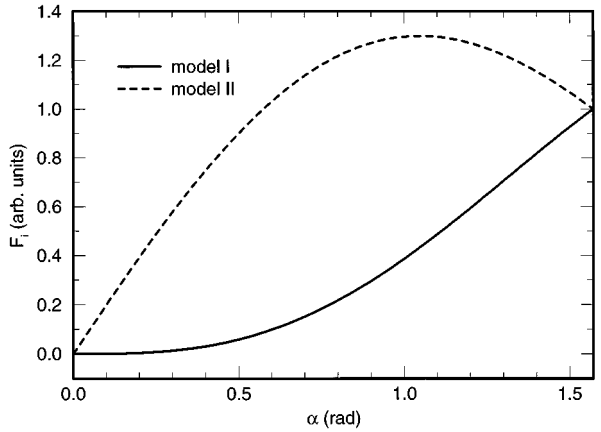

FIG. 22. Plot $F_i = f(\alpha)$ [Eq. (21)] showing the dependence of the bulk free energy on the angle α for the two models I and II. All other parameters are held constant.

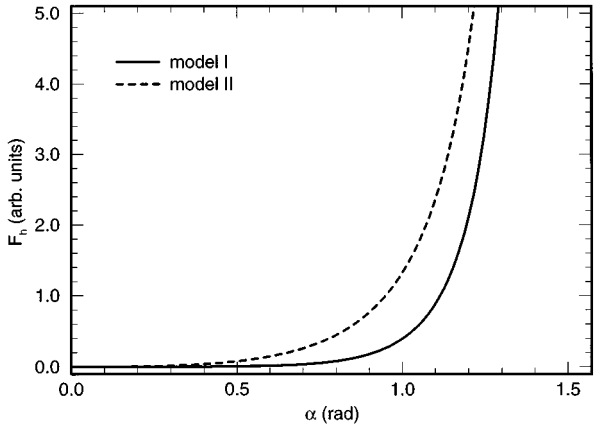

FIG. 24. Plot $F_h = f(\alpha)$ [Eq. (23)] showing the dependence of the free energy of the cone center on the angle α for the two models I and II. All other parameters are held constant.

with $\epsilon_{\mathrm{I}} = \alpha/2$ and $\epsilon_{\mathrm{II}} = (\pi - \alpha)/2$, respectively. The cone radius is r. Integrating over the volume of the cone, the area of its mantle and the length of the central defect line, we arrive at the following free energies:

$$F_{i,k} = 2k_i \sin^2 \alpha \tan \epsilon_k \{r[\ln(r/r_0) - 1] + r_0\}, \quad (21)$$

$$F_{c,k} = \pi k_c \frac{(1 - \sin \epsilon_k)^2}{\cos \epsilon_k \sin^2 \epsilon_k} r^2, \quad (22)$$

$$F_{h,k} = k_h \tan \epsilon_k \frac{(1 - \cos \alpha)^2}{\cos^2 \alpha} r. \quad (23)$$

The radius of the cone center is r_0. Plots of the deformation energies F_i, F_c, and F_h for the models I and II can be seen in Figs. 22, 23, and 24.

We conclude that $F_i \gg F_c + F_h$ because F_i is a bulk term and the two other terms concern regions of a much smaller volume. Experimentally we have the case $\alpha \neq 0$, so that all energies are finite; note also that the director distribution is continuous throughout the space. Therefore model I gives the lowest energy of all considered alternatives. But an undisturbed planar texture possesses nonetheless the lowest free energy. Thus there has to be a gain in free energy. This comes from the anchoring energy at the free surface. After integrating Eq. (2) over the surface area the free energy gives

$$F_f = -\pi k_f \cos^2(\pi/2 - \alpha - \xi_0) r^2. \quad (24)$$

The dependence on r is not the same for the appearing energies, so the angle of inclination should depend on r when calculated from the minimization process. However, this gives only a transcendental implicit expression that cannot be solved explicitly for α, even if only the absolutely necessary terms are taken into account. However, different values of α lead to different periodicities p_f of the relief at the free surface due to the cholesteric helix. Although we observe some variations for p_f, we do not see a statistically significant dependence on r. This leads to the conclusion that the surface anchoring is rather strong and determines the value of α, being $\alpha_0 = \pi/2 - \xi_0$. The variations in p_f are then attributed to the fact that none of the cones examined is really perfect. Our measurements give $\xi_0 = \arccos(p_0/p_f) = 37°$, $\alpha = 53°$, and $\epsilon_{\mathrm{I}} = 26°$. From the inequality $|F_f| > |F_i|$ we can calculate a lower boundary for k_f; using $r = 2500$ nm, $r_0 = p_0/4 = 73$ nm, and $k_i = 3 \times 10^{-7}$ dyne, results in $k_f > 6 \times 10^{-4}$ dyne cm^{-1}.

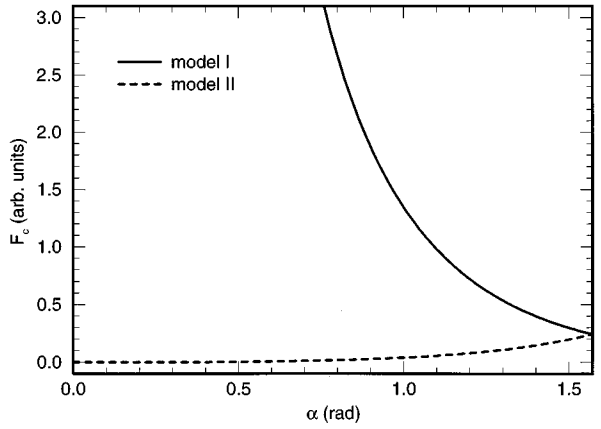

FIG. 23. Plot $F_c = f(\alpha)$ [Eq. (22)] showing the dependence of the cone border free energy on the angle α for the two models I and II. All other parameters are held constant.

Another consequence of the different dependences $F(r)$ is that the gain in free energy is greater when the domains become larger, thus they should increase with time. The growth stops only when the two domains meet. Another parameter that imposes a barrier for the domain radius is the thickness of the sample. When the bottom of the cone arrives at the other surface, the domain growth effectively stops, because the reorientation time for the director at this surface is of a much greater time scale. These considerations are indeed in agreement with the experimental findings (see Sec. III A).

A last estimation shall be made with respect to the height of the free surface cone. Still assuming that the surface anchoring is very strong, the bulk free energy F_i can be reduced by inclining the free surface, yielding a cone at the free surface. Neglecting gravitational terms, the free energy is given by (only taking the absolute necessary terms):

$$F = F_f + F_i \tag{25}$$

$$= \pi\sqrt{1+\tan^2\ \eta}(\gamma - k_f)r^2 + k_i\ \sin^2(\alpha_0 - \eta) \times \tan[(\alpha_0 - \eta)/2]r\ln(r/r_0), \tag{26}$$

where η is the surface cone angle and γ is the surface tension. Note that the factor $\cos^2(\pi/2-\alpha_0-\xi_0)$ of Eq. (24) is 1 for optimal anchoring. In order to get an approximation we develop the free energy in powers of η (up to second order) and minimize. This gives

$$\eta = \frac{2k_i(\cos\ \alpha - \cos 2\alpha)\ln(r/r_0)}{\pi(\gamma - k_f)r + k_i(2\sin 2\alpha - \sin\ \alpha)\ln(r/r_0)}. \tag{27}$$

To simplify the dependence $\eta(r)$ we neglect all terms of the denominator other than the first, which is considered to be predominant. Also taking into account $|\gamma| \gg |k_s|$, we can estimate the inclination angle. Using $\gamma = 40$ dyne cm^{-1} gives $\eta = 3\times10^{-3}$°. This value is too low compared with the experimental findings. Too many nonjustified assumptions have probably been made during the development of the approximation, especially that $F_i \gg F_c + F_h$. Including F_h in Eq. (25) will probably increase the angle η. Another point is that we have used values for monomeric substances in the absence of proper ones for our oligomeric material. Equation (27) is obtained by using only the predominant term of F_i for large radii. In this region $\eta(r)$ is a decaying function. Our experimental results, however, do not allow a definitive conclusion for this behavior, due to the great statistical variations.

G. Focal-conic domains

Defects appear in a layered system of parallel surfaces at those points where different layer normals cut each other. In the general case, these points construct surfaces. For energetical reasons, the system will develop a structure that minimizes the regions of defects. This gives the focal-conic texture, where defect surfaces degenerate to two curves, an ellipse, and a hyperbola. They pass through the focii of each other, the planes in which the two curves are located being perpendicular to one another. The local layer normal is always parallel to the unique straight line that cuts both the ellipse and the hyperbola [22].

In our case, the two defect curves are a circle and a straight line. The model cuts out a part of an infinite focal conic, which is sketched in Fig. 25. The defect line can be seen in the actual sample while the circle lies outside of the region that is covered by the domain. Therefore, the physical constraint for the layer normals to cut each other at the circle does no longer exist. This defect can relax to any surface, giving rise to a more general arrangement of the cholesteric planes. This is the concept of virtual focal surfaces [22].

However, the observed structure can nonetheless be described by a focal-conic arrangement. We have to increase the distance between the circle plane and our domain to infinity to arrive at straight lines for the layers sketched in Fig. 10. Note that we also have to increase the circle radius to infinity in order to maintain a constant cone angle α.

If we neglect the spiral arrangement of the cholesteric planes and consider only their conical arrangement, our idealized structure lies between two sorts of focal conics. Normally only focal conics of the first kind are observed, where the Gaussian curvature is negative; $\sigma_1\sigma_2 < 0$, σ_1^{-1}; and σ_2^{-1} are the radii of curvature. The layers have therefore a hyperbolic shape. But a second possibility for constructing a focal conic shows the inverse curvature $\sigma_1\sigma_2 > 0$; the layers have an elliptic shape [27]. The second kind is only very rarely observed [28]. In the ideal case, we have $\sigma_1\sigma_2 = 0$ (parabolic shape), but deviations from its structure may appear in both directions (see Fig. 26). Note, however, that a circular cone with constant slope angles η and ϵ and nonvarying $p_f(r)$ and $p_c(r)$ is only possible for $\sigma_1\sigma_2 = 0$. Thus the deviations from the ideal case cannot be very large, because we observe no variations either in $p_f(r)$ or in $\eta(r)$. In our model, $\sigma_1\sigma_2 = 0$ for the cholesteric planes in both the focal-conic and planar domains lead also to the vanishing of the Gaussian curvature for the domain border(s). The geometrical form of the surface focal-conic domains is therefore quite regular. In our opinion, this is due to the planar texture of the bulk that imposes ''clear'' conditions for the border and the central defects. Only once was a different spiral (fourfold) found. In all other cases we observed the usual double spiral.

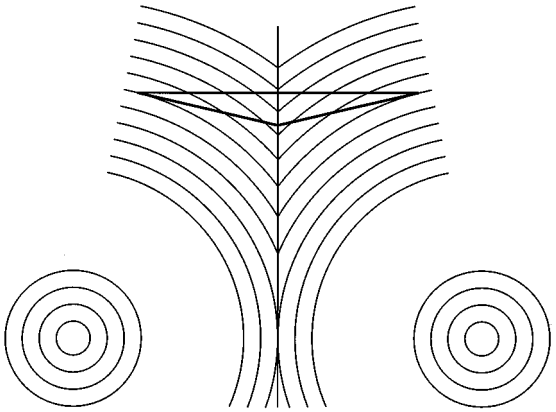

FIG. 25. Location of the cholesteric focal-conic domains at the free surface in relation to the general focal-conic structure.

In the general case, when two focal-conic domains meet, defects may appear on the border and the central defect lines

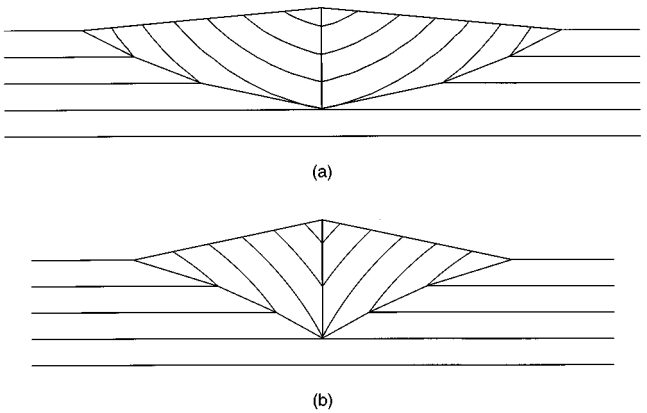

FIG. 26. Two sorts of deviations from the idealized structure. (a) The Gaussian curvature is positive. This curvature appears very seldom. (b) The Gaussian curvature is negative. Most of the focal-conic domains possess this sort of layer curvature.

may have different indices m and S, respectively. The periodicities along the surface between two domains can vary and the surface itself may possess a curvature $\sigma_1\sigma_2 \neq 0$.

V. CONCLUSION

In this article we have presented experimental material concerning AFM examinations of free surfaces and microtome cuts of an oligomeric cholesteric phase. The structure of the focal-conic domains that appear spontaneously at the free surface has been revealed. The cholesteric planes are inclined relative to the underlying bulk planar texture and have the form of a helicoidal cone. The structure shows no disclinations for **n**; only in the center of the cone, two λ^+ defects twist themselves around each other. There are no defects on the border between the focal-conic and the planar domains. The whole structure develops because the anchoring at the free surface favors an oblique orientation of the helix axis **t** relative to the surface. The focal-conic structure is the director distribution of least elastic energy which allows for this surface anchoring together with a bulk planar structure. The energy is further lowered by transforming the free surface to a cone with a small cone angle $\eta \sim 1°$, thus reducing the bulk distortion energy on costs of surface energy.

One more advantage of these focal conic domains is that they can develop locally. Alternative surface structures such as a linear texture need correlations between the cholesteric planes of dimensions much greater than in the case of the double spirals.

As the full height of the cone is rather small if not cut exactly in the center, it becomes clear why the focal-conic domains are only well visible in oblique cuts. Note also that the focal conic of Fig. 5 is not embedded in the planar texture as described by the model. The ''bend'' of the cholesteric planes (Fig. 13) is not the way the model predicts. We explain this by the fact that the domain border in this case is not focal-conic/planar but the one between two neighboring focal conic domains. This border has other conditions for the respective director distributions to fulfill. Let us note that we have indeed AFM images of perpendicular cuts where the embedding of the surface focal conic happens in the same way as in the model (see Fig. 7 for an oblique cut). However, in images of perpendicular cuts the focal-conic domains can rarely be seen due to their very small height.

ACKNOWLEDGMENTS

We would like to thank F. Livolant and co-workers for providing microtome instruments and cut technique. R. Meister is financially supported by the Postdoktorandenprogramm of the Deutsche Forschungsgemeinschaft.

[1] D. Sarid, *Scanning Force Microscopy with Applications to Electric, Magnetic and Atomic Forces* (Oxford University Press, Oxford, 1991).
[2] P. G. de Gennes, *The Physics of Liquid Crystals* (Clarendon Press, Oxford, 1974).
[3] T. Bertin-Mourot, Stage de FIUPSO, Université Paris Sud, 1994.
[4] B. D. Terris *et al.*, Phys. Lett. **19**, 85 (1992).
[5] H. Dumoulin and P. Pieranski (unpublished).
[6] M.-A. Hallé, Stage de ENS, Université Paris Sud, 1993.
[7] Y. Bouligand, J. Phys. (Paris) **34**, 603 (1973).
[8] Y. Bouligand, P. E. Cladis, L. Liebert, and L. Strzelecki, Mol. Cryst. Liq. Cryst. **25**, 233 (1974).
[9] F. Livolant and Y. Bouligand, Mol. Cryst. Liq. Cryst. **166**, 91 (1889).
[10] A. Leforestier and F. Livolant, Liq. Cryst. **17**, 651 (1994).
[11] T. J. Bunning *et al.*, Liq. Cryst. **16**, 769 (1994).
[12] H. Delacroix, J.-M. Gilli, I. Erk, and P. Mariani, Phys. Rev. Lett. **69**, 2935 (1992).
[13] D. W. Berreman, S. Meiboom, J. A. Zasadzinski, and M. J. Sammon, Phys. Rev. Lett. **57**, 1737 (1986).
[14] H. Dumoulin *et al.*, Mol. Cryst. Liq. Cryst. **262**, 221 (1995).
[15] M. Kamayé, Ph.D. thesis, Université de Nice—Sophia Antipolis, 1992 (unpublished).
[16] M. J. Stephen and J. P. Straley, Rev. Mod. Phys. **46**, 617 (1974).
[17] Y. Bouligand, J. Phys. (Paris) **35**, 215 (1974).
[18] J. Rault, in *Liquid Crystals and Ordered Fluids*, edited by J. F. Johnson and R. S. Porter (Plenum Press, New York, 1974), pp. 679–703.
[19] R. Meister, H. Dumoulin, M.-A. Hallé, and P. Pieranski, J. Phys. (France) II **6**, 827 (1996).
[20] P. E. Cladis and M. Kléman, Mol. Cryst. Liq. Cryst. **16**, 1 (1972).
[21] Y. Bouligand and M. Kléman, J. Phys. (Paris) **31**, 1041 (1970).
[22] M. Kléman, *Points, Lines and Walls* (John Wiley & Sons, New York, 1983).
[23] N. D. Mermin, Rev. Mod. Phys. **51**, 591 (1979).
[24] G. E. Volovik and W. P. Mineev, Zh. Eksp. Teor. Fiz. **72**, 2256 (1977) [Sov. Phys. JETP **45**, 1186 (1977)].
[25] J. Rault, Philos. Mag. **28**, 11 (1973).
[26] J. Rault, Philos. Mag. **30**, 621 (1974).
[27] Y. Bouligand, J. Phys. (France) **33**, 525 (1972).
[28] P. Boltenhagen, O. D. Lavrentovich, and M. Kléman, Phys. Rev. A. **46**, R1743 (1992).